Arsenic-Doped CdSeTe Solar Cells Achieve World Record 22.3% Efficiency

R. Mallick, X. Li, C. Reich, X. Shan, W. Zhang, T. Nagle, L. Bok, E. Bicakci, N. Rosenblatt, D. Modi, R. Farshchi, C. Lee, J. Hack, S. Grover, N. Wolf, W.K. Metzger, D. Lu, and G. Xiong

***Abstract*—For more than three decades, Cu has been critical to dope CdSeTe solar cells, form effective contacts, and maximize efficiency. At the same time, Cu defect chemistry has limited stability, carrier concentration, and further efficiency improvements. In this article, 22.3% world record efficiency is demonstrated without Cu by implementing As doping, which also improves stability, temperature coefficient, and energy yield. The efficiency crossing point of Group V technology relative to Cu has been driven by steady improvements in the open-circuit voltage. Here, the certified record cell reaches open-circuit voltage of 899 mV while retaining high photocurrent values of 31.4 mA/cm^2; the fill factor is relatively low at 78.9%. Coupling 80% fill factor with top open-circuit voltage values of 917 mV reported here offers a near-term path to 23% efficiency. Characterization indicates reducing recombination and improving activation provide viable paths to 25% efficiency.**

***Index Terms*—CdTe thin film solar cells, characterization of PV, semiconductor devices, solar energy.**

I. Introduction

CdSeTe solar technology has surpassed 50 GW of total deployment as its corresponding levelized cost of electricity has decreased below conventional fuels [1]. First Solar is projected to reach 20 GW annual production in just a few years [2]. For the past 30 years, production has used Cu to form effective back contacts and absorber doping to achieve high efficiency. However, the useful carrier concentration from Cu doping alone across diverse research institutions has been limited to mid-10^{14} cm^{-3} due to fundamental material carrier compensation limits that have contributed to a record efficiency plateau dating back to 2016 [3], [4], [5]. In addition, Cu can easily diffuse or migrate, thereby requiring careful doping control to achieve 30-year product lifetime [5], [6], [7], [8], [9].

Manuscript received 22 May 2023; revised 26 May 2023; accepted 31 May 2023. Date of publication 19 June 2023; date of current version 15 July 2023. *(Corresponding author: D. Lu.)*

The authors are with the California Technology Center, First Solar Inc., Santa Clara, CA 95050 USA (e-mail: rajni.mallick@firstsolar.com; xiaoping.li@firstsolar.com; carey.reich@firstsolar.com; xin.shan@firstsolar.com; wei.zhang@firstsolar.com; timothy.nagle@firstsolar.com; lisa.bok@firstsolar.com; evren.bicakci@firstsolar.com; nathan.rosenblatt@firstsolar.com; divyam.modi@firstsolar.com; rouin.farshchi@firstsolar.com; chungho.lee@firstsolar.com; jimmy.hack@firstsolar.com; sachit.grover@firstsolar.com; nathan.wolf@firstsolar.com; wyatt.metzger@firstsolar.com; dingyuan.lu@firstsolar.com; gxiong@firstsolar.com).

Color versions of one or more figures in this article are available at https://doi.org/10.1109/JPHOTOV.2023.3282581.

Digital Object Identifier 10.1109/JPHOTOV.2023.3282581

A shift to Group V (GrV) doping has offered a path to high carrier concentration, efficiency, and energy yield. Recent work demonstrated greater doping stability, a 100-fold increase in carrier concentration, and single-crystal V_{oc} greater than 1 V in 2016 [9], [10], [11], [12], [13], [14]. The greater stability is in part related to the slower diffusion of GrV dopants relative to Cu [15]. Implementing GrV dopants in polycrystalline CdSeTe solar cells did not immediately translate to improvements in either open-circuit voltage or efficiency [10], [16], [17], [18], [19], [20]. It is difficult for a relatively new technology to surpass longstanding and highly optimized processes.

In 2019, polycrystalline As-doped CdSeTe solar cells achieved open-circuit voltage of 857 mV [10]. More recent results indicated independently certified open-circuit voltage of 870 mV [21]. Here, we report certified results of 899 mV and internal results as high as 917 mV (Fig. 1) with an open-circuit voltage difference from band gap of 479 mV. The shift to As doping, which has overcome fundamental Cu-based defect chemistry limits to increase carrier concentration, has ultimately led to open-circuit voltage advances that have increased cell efficiency to a new record of 22.3%.

II. Experiment

The National Renewable Energy Laboratory (NREL) measured the current–voltage curve at 25 °C under 1000 W/m^2 ASTM global spectrum with its standard solar cell certification protocol. This included quantum efficiency (QE) measurements, spectral mismatch corrections, and aperture tests to rule out light piping. The cell area was determined to be 0.4491 cm^2 $\pm$ 0.2%.

Devices were fabricated on commercial soda-lime glass coated with fluorine-doped tin oxide. Vapor transport deposition was implemented to form a 3–4 μm $CdSe_xTe_{1-x}$ absorber layer. The samples were annealed in a $CdCl_2$-vapor environment between 400 °C and 500 °C. This introduces Cl at levels on the order of 10^{18} cm^{-3} and results in a graded CdSeTe layer with predominantly CdTe at the back surface. As was incorporated during absorber semiconductor fabrication. The back contact includes a thin ZnTe layer capped with a metal stack to form an electrode [10], [11]. An anti-reflection coating was added to the glass side to minimize frontside reflectance.

Capacitance-voltage (CV) characteristics were measured at different temperatures with an Agilent E4980A impedance analyzer. Voltage was scanned from -2 to $+0.5$ V in 0.1 V steps in

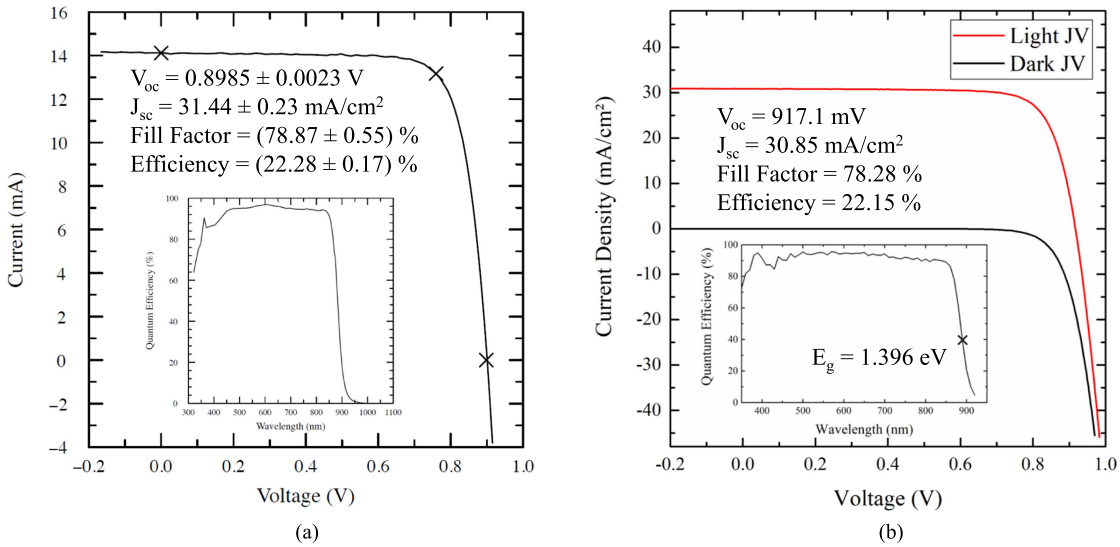

Fig. 1. (a) Current–voltage and quantum efficiency for 22.3% efficiency solar cell certified at NREL. (b) Current density–voltage and quantum efficiency for a solar cell with 917-mV V_{oc} measured at First Solar.

the dark, with a measurement frequency of 40 kHz. Electrochemical capacitance-voltage (ECV) characteristics were collected with a WEP Wafer Profiler CVP21, using dilute HCl in IPA to contact the back of the sample and the transparent conducting oxide to contact the front [22]. Voltage was scanned from 0.5 to −4.5 V in 0.15 V steps in the dark, with a measurement frequency of 2.3 kHz.

Bevels for cathodoluminescence (CL) measurements were prepared by focused-ion-beam milling in a Helios Nanolab 600i dual beam scanning electron microscope. A ∼1-μm-thick layer of protective Pt was deposited above the eventual beveled surface. The primary focused ion-beam mill was conducted at 30 kV to shape the bevel at 10°; afterwards, a low current was applied for a fine polish to remove curtaining effects. CL was collected with the Gatan Monarc system with electron-beam excitation conditions at 5 kV voltage and 1.5 nA current. To make false-color images, the CL spectrum of each pixel was fit with multiple Gaussians and the bandgap was determined from the high energy peak.

Time-resolved photoluminescence (TRPL) was measured by a PicoQuant Fluotime 300 spectrometer by applying time-correlated single photon counting [23], [24]. The laser excitation was a series of 640-nm laser pulses with 10^{13} photons/cm^2 incident either through the glass of fully completed devices or on the back of the CdSeTe absorber layer of partially formed devices. The external radiative efficiency (ERE) was measured with a constant white light-emitting diode source for 1-sun light bias and a low-excitation (<0.05 suns) 670-nm CW laser passed through a chopper for lock-in amplifier signal detection [25], [26].

Photoluminescence was detected by an InGaAs detector fitted with a long-pass filter. Diffuse 2% and 99% reflectance standards were used to calibrate the measurement to determine absolute ERE values. Secondary-ion mass spectrometry (SIMS) data were collected using a TOFSIMS-5 instrument with O_2-negative profiling.

III. Results

Fig. 1(a) illustrates the NREL current–voltage (IV) curve of the 22.3% As-doped cell. The curve indicates robust IV characteristics free of anomalies. The spectral QE in the inset of Fig. 1(a) shows low reflectance and parasitic absorption losses corresponding to the high short-circuit current density. The absence of CdS or similar intermediate bandgap buffers enables high current collection to wavelengths less than 400 nm. At the same time, the CdSeTe alloying enables current collection extending to wavelengths greater than 850 nm. The open-circuit voltage (V_{oc}) of 899 mV is among the highest values reported in polycrystalline CdSeTe, and it is a key enabler for the record cell efficiency of 22.3%. The fill factor of 78.9% is lower than the previous record cell and partially due to higher series resistance [21]. Fig. 1(b) shows the JV and QE curves of a device with V_{oc} of 917 mV. This device demonstrates a V_{oc} deficiency from the bandgap of 479 mV, which is the smallest among all published CdSeTe devices. Combining 917 mV V_{oc} and a fill factor of 80% provides a path toward 23% efficiency. In addition, the higher carrier concentration from As doping provides a platform for further increases toward 25% efficiency [13], [27]. The increase in efficiency using As doping is accompanied by greater long-term stability and relatively better high-temperature performance than Cu-based solar cells [11], [21].

Fig. 2(a) illustrates representative CV curves as a function of temperature. The measured net carrier concentration is given by the acceptor density subtracted by the donor density. At room temperature, it is 1–2 × 10^{16} cm^{-3} at zero bias and varies little as the depletion width is increased in reverse bias. Because CdSeTe can form complex defects and compensation, it is plausible that deep defects could be manifested in net carrier concentration changes with temperature. However, Fig. 2(a) illustrates that the defect chemistry does not indicate any appreciable freeze-out over the measured temperature range. This is consistent with shallow dopant states and As substituting on Te sites,

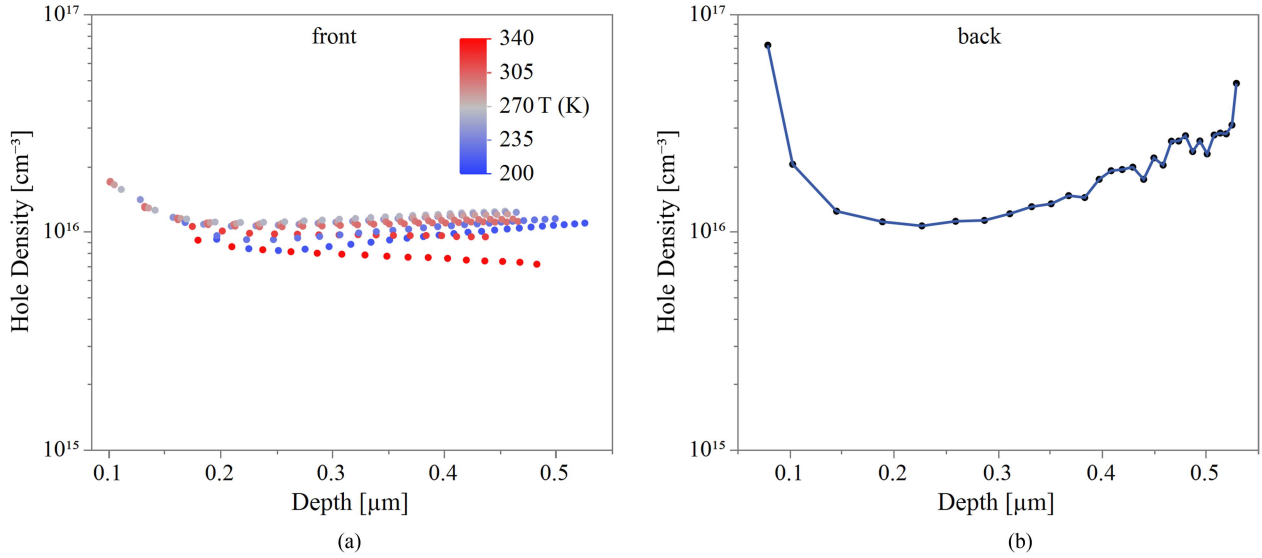

Fig. 2. (a) Capacitance-voltage data indicating net acceptor density vs. depletion width at the front interface as a function of temperature and (b) electrochemical capacitance-voltage data indicating net acceptor density as a function of depletion width at the back surface of the CdSeTe absorber.

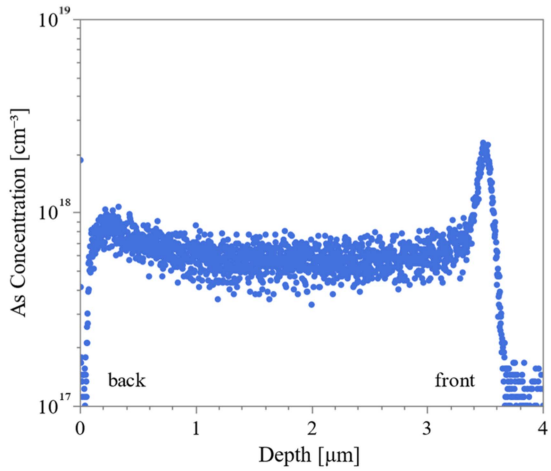

Fig. 3. SIMS As profile vs. absorber depth from back to front interface.

which is observed in photoluminescence and CL spectra [9], [10], [28].

Fig. 2(b) shows an electrochemical capacitance voltage (ECV) curve at room temperature. ECV is used to probe the carrier concentration at the back of the device by forming a semiconductor-electrolyte junction there that dominates the total capacitance response for select frequencies and voltages [22], [29]. Though the ECV data are noisier, the measurements indicate that the carrier concentration is similar (1–2 $\times$ 10^{16} cm^{-3}) in the back and front absorber regions. While neither frontside nor backside measurements penetrate throughout the entire absorber, the agreement in magnitude suggests the average carrier concentration is similar across the depth of the absorber layer.

Fig. 3 illustrates the arsenic concentration as measured by SIMS through the absorber layer of the completed device. The As concentration is approximately 5–6 $\times$ 10^{17} cm^{-3} in the bulk of the absorber away from the interfaces, corresponding to an activation ratio of $\sim$2% to 3%. A large As spike can be seen at the front interface. X-ray photoelectron spectroscopy and SIMS (not shown) after cleaving the front interface indicate As accumulation above 0.5% levels immediately adjacent to the transparent conducting oxide and little or no accumulation at the front adjacent to the absorber. This is consistent with oxidative segregation of As catalyzed by tin oxide [30], [31]. The degree that this may impact performance is not clear. Here, cells are still able to achieve high open-circuit voltage.

Fig. 4(a) illustrates photoluminescence decay curves collected by time-correlated single photon counting. The average lifetime is 5.7 ns, with τ_2 and τ_3 components of 11 and 52 ns, respectively. The average lifetime is 80% greater than results with 857 mV presented in 2019, while the carrier concentration is about the same, so it is plausible that increased lifetime has contributed to greater open-circuit voltage. Yet, the lifetime remains orders of magnitude less than state-of-the-art GaAs, $CuInGaSe_2$, and perovskites, indicating substantive room for future improvement [32], [33], [34], [35]. Fig. 4(b) illustrates the same measurements performed on the film side of sister samples. Characteristic of CdTe in general, the decay is much faster than the front side. The deconvoluted average decay time is 180 ps. Such short decay times have been observed on the back of the CdTe polycrystalline absorber across many institutions for decades and indicate another fundamental material challenge. Modeling and analysis indicate that this recombination velocity is not significantly limiting open-circuit voltage, however, it can cap future efficiency gains as absorber quality is improved, and it already is a key obstacle to achieving high bifaciality when transparent contacts are applied. Consequently, back surface passivation is an intensive area of research. In double heterostructures, effective back surface passivation has been achieved with alumina or other oxides, such as MgZnO. The $CdCl_2$ treatment with the back contact present is critical to

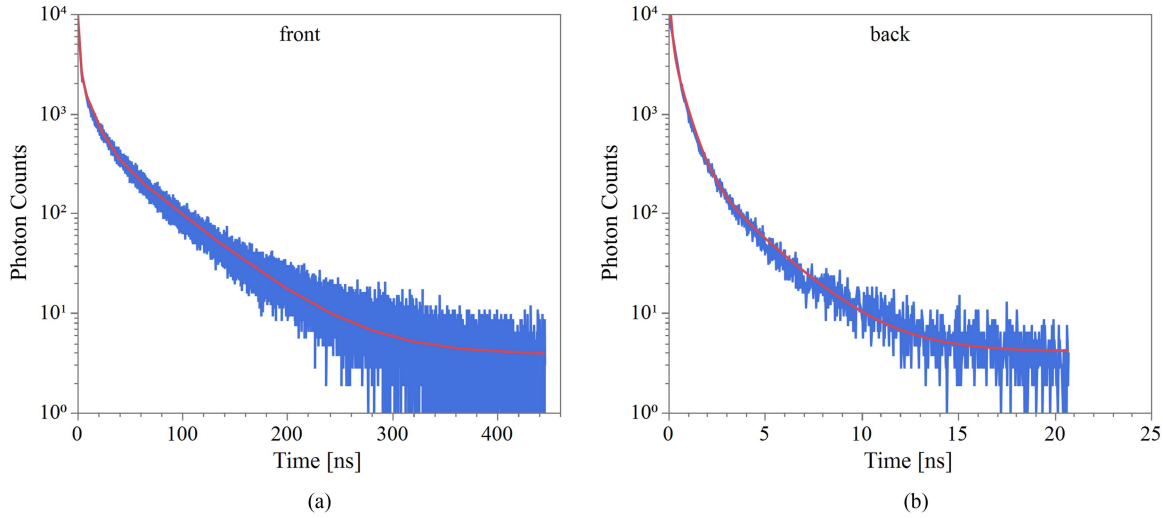

Fig. 4. Time-resolved photoluminescence decay curves (blue) and triexponential fit (red) measured (a) through the glass on completed device and (b) on the back of the CdSeTe absorber layer in a partially completed device.

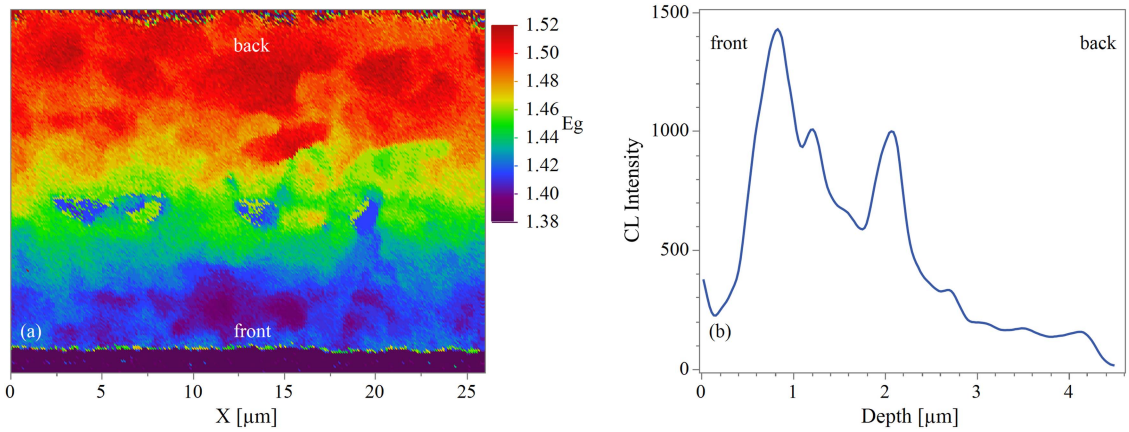

Fig. 5. (a) Bandgap across bevel derived from CL peak fitting and (b) average horizontal CL intensity as a function of depth from the front interface.

achieve this passivation [36], [37], [38]. Here, ZnTe is used as the back contact, which is well aligned with the CdTe valence band [39]. However, the ZnTe is not exposed to $CdCl_2$ because it is not compatible due to the formation of $ZnCl_2$ [40]. Future work may benefit from implementing different back contact materials exposed to $CdCl_2$ treatments to passivate the back surface.

Fig. 5(a) indicates the CL on beveled material adjacent to the record cell. The graded bandgap, taken from the peak emission energy, varies from approximately 1.4 eV at the front of the cell to 1.5 eV near the back. The lifetime varies systematically with the Se level. This is observed in experiments where Se level is varied (not shown), and it is manifested in the bevel, where the spectrally integrated room-temperature CL intensity in Fig. 5(b) decreases from front to back. Consequently, whereas the average carrier concentration appears to not vary appreciably as a function of depth based on CV and ECV, the lifetime decreases systematically as a function of distance from the front interface throughout the absorber.

The front-side ERE for these samples is 0.1%. Computational modeling indicates that the ERE values are consistent with 1×10^{16} carrier concentrations and an average lifetime of 5–10 ns. Fig. 6 shows the decreases from the ERE analysis from the Shockley–Quessier limit. The ideal V_{oc} based on the emission spectrum corresponds to 1.10 V. The implied V_{oc} indicates nonradiative recombination reduces the attainable V_{oc} by 180 to 920 mV. This is consistent with the lifetime measurements relative to the radiative recombination limit of 1 μs at 10^{16} cm^{-3} hole density levels. The 21-mV difference between implied V_{oc} and the measured V_{oc} indicates high carrier selectivity with some but relatively limited room for improvement [25]. While this may at first seem contradictory to the 78.9% fill factor values, reducing series resistance and differences between internal and external measurements can enable >80% fill factor, and these do not factor into ERE measurements. The TRPL and ERE data indicate 180 mV in V_{oc} and substantive corresponding efficiency gains are possible by improving carrier lifetime to much higher values. In fact, by increasing Se levels in the CdSeTe absorber,

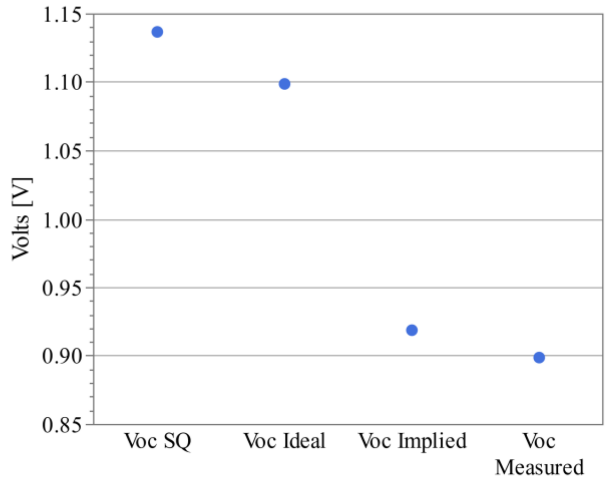

Fig. 6. Shockley–Quessier, ideal, implied, and measured V_{oc} determined from ERE analysis and device measurements.

we have demonstrated >1% ERE for $CdCl_2$ -treated absorbers before back contact deposition and >0.4% ERE for finished devices. The latter leads to implied V_{oc} beyond 940 mV, thereby significantly increasing headroom for further V_{oc} improvement.

Relative to earlier results that achieved 857 mV [10], here the carrier concentration is similar and recombination is less. Other contributing factors to performance are inhomogeneity and electrostatic fluctuations. As has been demonstrated to form electrostatic fluctuations [10], [41]. These fluctuations are proportional to the total acceptor and donor density [41]. A two-fold reduction in As incorporation level is sufficient by analytical estimates to describe a 40–50 mV increase in open-circuit voltage.

In single crystals, it is possible to achieve 50% activation [13], [14], [42]. However, here and throughout the community, chlorinated polycrystalline films remain limited to several percent activation [10], [19], [20]. Consequently, a path for further improving performance is to enhance activation by modifying the As and Cl defect chemistry or by using different dopants.

Carrier lifetime can be increased with increasing Se levels, but this also tends to shift the equilibrium Fermi less p-type. Consequently, increasing Se in practice will often incur tradeoffs in activation and carrier concentration, limiting the ability to increase hole density and lifetime simultaneously to achieve greater efficiency. In parallel, attempting to dope high Se regions with increasing dopant levels due to decreasing activation can induce greater voltage losses from electrostatic fluctuations. Further work is needed to better understand, characterize, and manipulate CdSeTe defect chemistry to advance the technology.

IV. Conclusion

We demonstrate record cell efficiency of 22.3% using arsenic doping. This represents the first CdSeTe record solar cell that has not used Cu. The eventual shift in record technology has been driven by the steady increase in open-circuit voltage to values now reaching and exceeding the 900-mV mark, which brings the V_{oc} to bandgap deficit below 500 mV. Stable higher carrier concentration has helped achieve this. Coupling fill factor greater than 80% with recent open-circuit voltage values of 917 mV offers a near-term path to 23% efficiency. Characterization and analysis indicate that improving recombination and activation provide viable paths to increase efficiency toward 25%.

References

[1] "Levelized cost of energy and levelized cost of storage—Version 15.0, lazard," Oct. 2021. [Online]. Available: https://www.lazard.com/media/sptlfats/lazards-levelized-cost-of-energy-version-150-vf.pdf
[2] 2023. [Online]. Available: https://www.firstsolar.com/
[3] "Best research cell efficiency chart," 2023. [Online]. Available: https://www.nrel.gov/pv/cell-efficiency.html
[4] J. Ma, S.-H. Wei, T. A. Gessert, and K. K. Chin, "Carrier density and compensation in semiconductors with multiple dopants and multiple transition energy levels: Case of Cu impurities in CdTe," *Phys. Rev. B*, vol. 83, 2011, Art. no. 245207.
[5] D. Krasikov and I. Sankin, "Defect interactions and the role of complexes in CdTe solar cell absorber," *J. Mater. Chem. A*, vol. 5, pp. 3503–3513, 2017.
[6] D. Grecu and A. D. Compaan, "Photoluminescence study of Cu diffusion and electromigration in CdTe," *Appl. Phys. Lett.*, vol. 75, pp. 361–363, 1999.
[7] D. Grecu, A. D. Compaan, D. Young, U. Jayamaha, and D. H. Rose, "Photoluminescence of Cu-doped CdTe and related stability issues in CdS/CdTe solar cells," *J. Appl. Phys.*, vol. 88, pp. 2490–2496, 2000.
[8] C. Gretener et al., "New, perspective on the performance stability of CdTe solar cells," *Sol. Energy Mater. Sol. Cells*, vol. 146, pp. 51–57, 2016.
[9] J. M. Burst et al., "Carrier density and lifetime for different dopants in single crystal and polycrystalline CdTe," *Appl. Phys. Lett. Mater.*, vol. 4, 2016, Art. no. 116102.
[10] W. K. Metzger et al., "Exceeding 20% efficiency with in situ group V doping," *Nature Energy*, vol. 4, pp. 837–845, 2019.
[11] D. Krasikov, D. Guo, S. Demtsu, and I. Sankin, "Comparative study of As and Cu doping stability in CdSeTe absorbers," *Sol. Energy Mater. Sol. Cells*, vol. 224, 2021, Art. no. 111012.
[12] J. N. Duenow et al., "Single-crystal CdTe solar cells with V_{oc} greater than 900 mV," *Appl. Phys. Lett.*, vol. 105, 2014, Art. no. 053903.
[13] J. M. Burst et al., "CdTe solar cells with open-circuit voltage breaking the 1 V barrier," *Nature Energy*, vol. 1, 2016, Art. no. 16015.
[14] A. Nagaoka, D. Kuciauskas, D. McCoy, and M. A. Scarpulla, "High p-type doping, mobility and photocarrier lifetime in arsenic-doped CdTe single crystals," *Appl. Phys. Lett.*, vol. 112, 2018, Art. no. 192101.
[15] E. Colegrove et al., "Experimental and theoretical comparison of Sb, As and P diffusion mechanisms and doping in CdTe," *J. Phys. D Appl. Phys.*, vol. 51, 2018, Art. no. 075102.
[16] T. L. Chu, S. S. Chu, C. Ferekides, J. Britt, and C. Q. Wu, "Thin-film junctions of cadmium telluride by metalorganic chemical vapor deposition," *J. Appl. Phys.*, vol. 71, 1992, Art. no. 3870.
[17] R. A. Berrigan, N. Maugn, S. J. C. Irvine, D. J. Cole-Hamilton, and D. Ellis, "Thin films of CdTe/CdS grown by MOCVD for photovoltaics," *J. Cryst. Growth*, vol. 195, pp. 718–724, 1998.
[18] Y. Y. Proskuryakov et al., "Doping levels, trap density of states and the performance of co-doped CdTe(As,Cl) photovoltaic devices," *Sol. Energy Mater. Sol. Cells*, vol. 93, pp. 1572–1581, 2009.
[19] G. Kartopu et al., "Study of thin film poly-crystalline CdTe solar cells presenting high acceptor concentrations achieved by in-situ arsenic doping," *Sol. Energy Mater. Sol. Cells*, vol. 194, pp. 259–267, 2019.
[20] B. E. McCandless et al., "Overcoming carrier concentration limits in polycrystalline CdTe thin films with in-situ doping," *Sci. Rep.*, vol. 8, 2018, Art. no. 14519.
[21] W. K. Metzger et al., "As-doped CdSeTe solar cells achieving 22% efficiency with −0.23%/°C temperature coefficient," *IEEE J. Photovolt.*, vol. 12, no. 6, pp. 1435–1438, Nov. 2022.
[22] N. Rosenblatt, A. Polizzotti, S. Grover, X. Li, and W. K. Metzger, "Measuring carrier concentration on the back side of thin film solar cells," in *Proc. IEEE 49th Photovolt. Specialists Conf.*, 2022, pp. 1355–1357.
[23] D. V. O'Connor and D. Phillips, *Time-Correlated Single Photon Counting*. New York, NY, USA: Academic Press, 1984.
[24] W. K. Metzger et al., "Time-resolved photoluminescence studies of CdTe solar cells," *J. Appl. Phys.*, vol. 94, pp. 3549–3555, 2003.

[25] A. Onno, C. Chen, P. Koswatta, M. Boccard, and Z. C. Holman, "Passivation, conductivity, and selectivity in solar cell contacts: Concepts and simulations based on a unified partial-resistances framework," *J. Appl. Phys.*, vol. 126, 2019, Art. no. 183103.
[26] A. Onno et al., "Understanding what limits the voltage of polycrystalline CdSeTe solar cells," *Nature Energy*, vol. 7, pp. 400–408, 2022.
[27] A. Kanevce, M. O. Reese, T. M. Barnes, S. A. Jensen, and W. K. Metzger, "The roles of carrier concentration and interface, bulk, and grain-boundary recombination for 25% efficient CdTe solar cells," *J. Appl. Phys.*, vol. 121, 2017, Art. no. 214506.
[28] S. Grover et al., "Characterization of arsenic doped CdTe layers and solar cells," in *Proc. IEEE 44th Photovolt. Specialist Conf.*, 2017, pp. 1193–1195.
[29] A. Niemegeers and M. Burgelman, "Effects of the Au/CdTe back contact on IV and CV characteristics of Au/CdTe/CdS/TCO solar cells," *J. Appl. Phys.*, vol. 81, no. 6, pp. 2881–2886, 1997, doi: 10.1063/1.363946.
[30] C. L. Perkins, B. McCandless, D. L. McGott, M. O. Reese, and W. Metzger, "Oxidative segregation of group V dopants in CdTe solar cells," in *Proc. IEEE 46th Photovoltaic Specialists Conf.*, 2019, pp. 0169–0172.
[31] C. L. Perkins, D. L. McGott, M. O. Reese, and W. K. Metzger, "SnO_2-catalyzed oxidation in high-efficiency CdTe solar cells," *Amer. Chem. Soc. Appl. Mater. Interfaces*, vol. 11, pp. 13003–13010, 2019, doi: 10.1021/acsami.9b00835.
[32] W. K. Metzger, I. L. Repins, and M. A. Contreras, "Long lifetimes in high-efficiency Cu(In,Ga)Se2 solar cells," *Appl. Phys. Lett.*, vol. 93, 2008, Art. no. 022110.
[33] D. W. deQuilettes et al., "Impact of microstructure on local carrier lifetime in perovskite solar cells," *Science*, vol. 348, pp. 683–686, 2015.
[34] H. C. Casey and F. Stern, "Concentration-dependent absorption and spontaneous emission of heavily doped GaAs," *J. Appl. Phys.*, vol. 47, 1976, Art. no. 631.
[35] G. B. Lush et al., "Microsecond lifetimes and low interface recombination velocities in moderately doped n-GaAs thin films," *Appl. Phys. Lett.*, vol. 61, pp. 2440–2442, 1992.
[36] J. M. Kephart et al., "Sputter-deposited oxides for interface passivation of CdTe photovoltaics," *IEEE J. Photovolt.*, vol. 8, no. 2, pp. 587–593, Mar. 2018.
[37] D. Kuciauskas et al., "Recombination velocity less than 100 cm/s at polycrystalline Al_2O_3/CdSeTe interfaces," *Appl. Phys. Lett.*, vol. 112, 2018, Art. no. 263901.
[38] M. Amarasinghe et al., "Mechanisms for long carrier lifetime in CdSeTe double heterostructures," *Appl. Phys. Lett.*, vol. 118, 2021, Art. no. 211102.
[39] B. Spaith, J. Fritsche, A. Klein, and W. Jaegerman, "Nitrogen doping of ZnTe and its influence on CdTe/ZnTe interfaces," *Appl. Phys. Lett.*, vol. 90, 2007, Art. no. 062112.
[40] D. E. Swanson et al., "$CdCl_2$ passivation of polycrystalline CdMgTe and CdZnTe absorbers for tandem photovoltaics cells," *J. Appl. Phys.*, vol. 123, 2018, Art. no. 203101.
[41] J. Moseley et al., "Impact of dopant-induced optoelectronic tails on open-circuit voltage in arsenic-doped Cd(Se)Te solar cells," *J. Appl. Phys.*, vol. 128, 2020, Art. no. 103105.
[42] S. Farrell et al., "Arsenic doping of CdTe/Si by molecular beam epitaxy," *J. Electron. Mater.*, vol. 44, pp. 3202–3206, 2015.